OPEN ACCESS

University of BRISTOL

Publisher's PDF, also known as Version of record

Link to published version (if available):
10.1063/1.5040100

Link to publication record in Explore Bristol Research
PDF-document

University of Bristol - Explore Bristol Research
General rights

Chao Yuan, James W. Pomeroy ⓘⓓ, and Martin Kuball

COLLECTIONS

ⓔⓟ   This paper was selected as an Editor's Pick

View Online   Export Citation   CrossMark

ARTICLES YOU MAY BE INTERESTED IN

Acceptor doping of β-Ga_2O_3 by Mg and N ion implantations
Applied Physics Letters **113**, 102103 (2018); https://doi.org/10.1063/1.5050040

GaN surface as the source of non-radiative defects in InGaN/GaN quantum wells
Applied Physics Letters **113**, 111106 (2018); https://doi.org/10.1063/1.5048010

Leakage mechanisms in GaN-on-GaN vertical pn diodes
Applied Physics Letters **112**, 233501 (2018); https://doi.org/10.1063/1.5033436

Above bandgap thermoreflectance for non-invasive thermal characterization of GaN-based wafers

Chao Yuan,[a] James W. Pomeroy, and Martin Kuball
Center for Device Thermography and Reliability (CDTR), H. H. Wills Physics Laboratory, University of Bristol, BS8 1TL Bristol, United Kingdom

GaN devices integrated with dissimilar substrates have transformed electronic and optoelectronic applications. However, an effective thermal resistance (TBR_eff) exists between the GaN layer and the dissimilar substrates typically, which can potentially cause a major heat transport bottleneck. A non-invasive method for monitoring the TBR_eff of bare wafers is a key enabler for process monitoring and for the reduction of TBR_eff through design optimization. The existing TBR_eff measurement techniques require metal deposition on the sample surface. Here, we demonstrate a generic non-invasive transient thermoreflectance technique which does not require modification of the GaN surface and can be applied to any GaN-based wafers, regardless of the substrate material. Above-bandgap pump and probe lasers are used to avoid any interference caused by sub-surface reflections, ensuring that this technique strictly follows the fundamental principle of thermoreflectance-based methods. Several GaN wafers on common substrates (SiC, Si, diamond, and sapphire) are measured to assess the validity of this technique. *Published by AIP Publishing.* https://doi.org/10.1063/1.5040100

GaN devices have transformed electronic and optoelectronic applications, including high-power radio frequency (RF) amplifiers, power electronics, light-emitting diode (LED) devices, and laser diodes, enabling more compact devices with higher operating power densities than were previously possible.[1,2] Thermal management is the key to enabling reliable high-power operation, allowing for efficient extraction of waste heat from the active part of the device. The majority of GaN devices feature some form of heterogenous integration with dissimilar substrates, for example, heteroepitaxy on high thermal conductivity SiC is common for high-power RF amplifiers.[3] More recently, GaN-on-diamond processes have been developed, based on wafer bonding or direct diamond growth, taking advantage of the extremely high thermal conductivity of diamond.[4–7] Integrating GaN devices with silicon CMOS is another active research topic.[8] However, heterogeneous integration can pose a major thermal management bottleneck when a potentially significant effective thermal boundary resistance (TBR_eff) is present between the GaN layer and the substrate. The TBR_eff is associated with the nucleation/bonding interface, which is within a micron length scale of the region where heat is generated in the device channel.[9,10] TBR_eff can be reduced by optimising the growth/bonding process and would ideally be routinely monitored by screening wafers in production.

Existing TBR_eff measurement techniques include Raman thermography,[7] which, however, requires device fabrication. Thermoreflectance-based techniques, e.g., time-domain thermoreflectance (TDTR)[11,12] and transient thermoreflectance (TTR),[13–16] have emerged as powerful techniques to measure the thermal properties and TBR_eff of layered structures. Both TDTR and TTR are pump-probe techniques in which a pulsed pump heats the surface of a thin-film metal transducer deposited on the sample; the probe beam monitors the surface temperature response via the induced change in reflectivity. The metal transducer used for the TDTR and TTR techniques

ensures that heating occurs at the surface. The metal thermo-optic coefficient is linear, meaning that the measured change in reflectivity is proportional to the change in surface temperature, which is the basis of pump-probe thermoreflectance techniques. Figure 1(a) shows a schematic of conventional metal-transducer TTR measurement configuration, in which the nanosecond pump laser heats a thin-film metal transducer deposited on the sample. The measurement time range is from nanoseconds to microseconds, with the photodiode transimpedance amplifier being the main bandwidth limiting component.[14,15] In comparison, TDTR typically uses a picosecond pump and probe laser with a mechanical optical delay stage, which limits the maximum measurement time window to around 10 ns.[11,12] A long measurement range is preferable to GaN heteroepitaxy given the thermal relaxation time of the layer structure is up to microseconds.[10] However, the drawback of these techniques is that using a metal transducer makes the testing destructive—it cannot be used in production.

A transducer-less TTR technique was demonstrated in year 2014 which enables measurements to be performed on GaN-on-diamond wafers directly,[17] enabling thermal resistance characterisation before subsequent device fabrication. This technique uses a 10 ns above-GaN bandgap pump laser (355 nm, 3.49 eV) to directly heat the GaN surface, as illustrated in Fig. 1(b). This exploits GaN strong optical absorption, with an absorption depth (d) of about 100 nm ($d = 1/a$, where a is the absorption coefficient, which is 10^5 cm^{-1} at 355 nm)[18] in GaN at the pump wavelength. A below-bandgap continuous wave (CW) 532 nm laser probes the Fresnel reflection, modulated by the temperature dependent refractive index (n); the thermo-optic coefficient dn/dT of GaN at room temperature is 10^{-4} K^{-1} at 532 nm.[19] This above-bandgap pumping below-bandgap probing transducer-less TTR is referred here as transducer-less UV/Vis-TTR. In the case of AlGaN/GaN-on-diamond, the dominant reflection is at the AlGaN/GaN surface where the refractive index contrast is the largest ($\Delta n_{air/GaN} \sim 1.4$, $\Delta n_{GaN/Diamond} \sim 0.02$ at 532 nm),

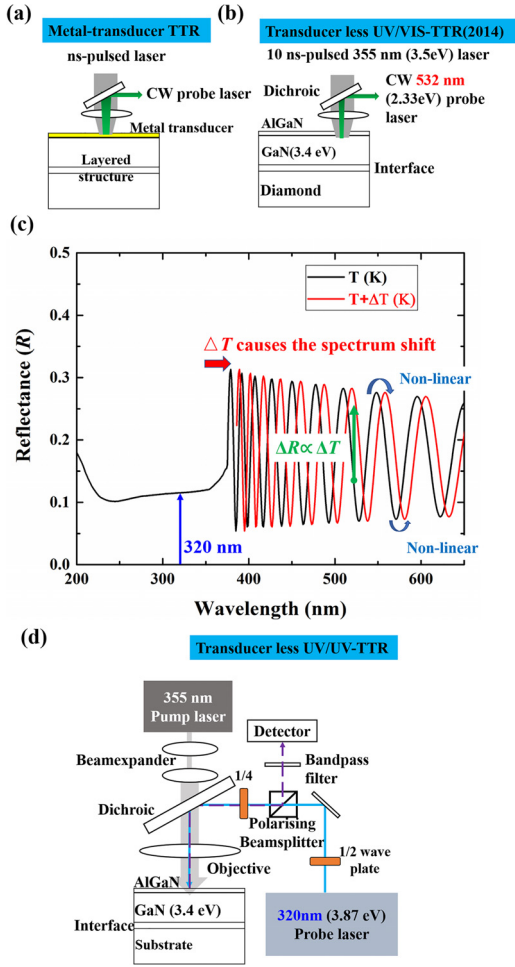[a] Electronic mail: cy17772@bristol.ac.uk

FIG. 1. (a) Schematic of the standard metal-transducer TTR measurement configuration, in which the nanosecond pump laser heats a thin-film metal transducer deposited on the sample. (b) Schematic of the transducer-less UV/Vis-TTR described in Ref. 17, in which an above-bandgap 10 ns pump laser directly heats the GaN surface. (c) Calculated Fresnel reflectivity spectrum from 200 nm to 650 nm for a AlGaN(20 nm)/GaN (1300 nm)-SiN$_x$(50 nm)-diamond wafer and the illustration of the shift of the interference pattern induced by a temperature rise (ΔT). (d) Schematic of the transducer-less UV/UV-TTR measurement configuration, which uses the above-bandgap lasers for both GaN surface heating and probing.

making this measurement most sensitive to AlGaN/GaN surface temperature changes. However, challenges arise due to the GaN/substrate reflections that may contribute to the total reflectance, resulting in interference fringes in the reflectance spectrum, illustrated for an AlGaN/GaN-on-diamond wafer in Fig. 1(c). Since the refractive index is a function of both temperature[19] and wavelength,[20] ideally, as shown in Fig. 1(c), a temperature increase (ΔT) is equivalent to a shift in reflectance spectrum. Measuring the reflectance at a wavelength that lies far from the interference extrema, a linear temperature dependence can be observed, as indicated in Fig. 1(c). However, the position of the extrema depends on the refractive indices and thicknesses of the layers in the structure. In some cases, where the probe laser wavelength is close to the interference fringe minima or maxima, the reflectivity response may not be linearly related to the surface temperature change. In addition, this technique can also not be applied when there is a large refractive index contrast between the GaN layer and substrates, e.g., sapphire or Si substrate ($\Delta n_{GaN/sapphire} \sim 0.6$, $\Delta n_{GaN/Si} \sim 1.75$), because the dominant

reflection of probe light is from the GaN/substrate interface, rather than the surface. We notice that avoiding sub-surface reflections altogether would avoid any possible measurement artifacts. This brings in the motivation that replacing the 532 nm probe laser with an alternative probe laser overcomes the sub-surface reflection challenge.

We achieved this by using a CW above-bandgap 320 nm ultraviolet (UV) probe laser, rather than below-bandgap, to monitor the surface reflectivity. At this wavelength, the absorption depth (d) is about 80 nm ($d = 1/a$, $a \sim 125 \times 10^5$ cm^{-1} at 320 nm),[18] preventing sub-surface reflections for typical GaN layer thicknesses. This makes the technique truly generic and can be applied to any GaN layer, regardless of the substrate material.

Here, we introduce the TTR technique which uses the above-bandgap lasers for both GaN surface heating and probing. We refer to this technique as transducer-less UV/UV-TTR. Figure 1(d) shows the schematic of measurement configuration. As with the previously developed transducer-less UV/Vis-TTR,[17] the pump beam is a 355 nm (3.49 eV) frequency tripled Nd:YAG laser with a 30 kHz repetition rate. After passing through a beam expander and a dichroic beam splitter, it is directed through a 15×0.3 N.A. quartz objective (LMU-15X-NUV, Thorlabs) onto a de-focused spot in the sample with a 50 μm FWHM Gaussian profile and a 10 ns laser pulse. The pump laser power incident on the sample surface is less than 10 mW (time averaged, peak: 30 W). The transient surface reflectivity change is monitored using a 320 nm (3.87 eV) UV laser probe beam, focused on the sample surface. The probe laser power incident on the sample surface is around $\sim$1 mW, much less than that of the pump, avoiding heating of the surface. The reflected beam intensity is sampled by a polarising beam splitter and detected by a silicon amplified photodetector (0.18A/W responsibility, 7 ns rise time, 50 MHz bandwidth, PDA8A/Thorlab) and a digital oscilloscope (300 MHz bandwidth). To ensure no residual light from the pump beam or photoluminescence is detected, a 320 nm bandpass filter with a 10 nm FWHM is placed before the detector.

Several GaN wafers on common substrates were measured: GaN-on-SiC, GaN-on-sapphire, GaN-on-Si and two GaN-on-diamond wafers. Table I provides the details of sample structure. The GaN-on-diamond layer structure consists of a GaN epilayer and a thin SiN$_x$ dielectric on a CVD grown polycrystalline diamond substrate. The only difference between the two GaN-on-diamond wafers is the dielectric layer thickness: 50 nm and 90 nm. More details about these two wafers are given in Ref. 17. The other wafers were

TABLE I. Structure information of the investigated samples.

Wafers	GaN thickness (μm)	Interlayer thickness (μm)	Substrate thickness (μm)
GaN-90 nm SiN$_x$-diamond	0.7	0.09	110
GaN-50 nm SiN$_x$-diamond	0.7	0.05	110
GaN-on-SiC	1.67	0.03	300
GaN-on-sapphire	1.8	0.08	300
GaN-on-Si	0.2	0.94	500

GaN epilayers deposited on insulating 4H-SiC (0001) and sapphire (0001) substrates, respectively, using a thin AlN nucleation layer. For the GaN-on-Si (111) wafer, the structure includes a strain relief layer (SRL) between GaN and Si, which consists of several layers of AlGaN with unknown Al composition. All the samples have a 20–30 nm-thick AlGaN layer (forming the AlGaN/GaN heterostructure) on top with the Al composition between 20% and 25%. At this composition, the AlGaN layer is transparent at both the pump and probe wavelengths. Figure 2(a) shows the measured thermoreflectance transients, normalized to the peak reflectivity modulation. All the samples were tested at an ambient temperature of 25 °C.

Since the AlGaN layer thickness is much less than the probe wavelength, there is no interference fringe between 230 nm and 360 nm, as evident in the reflectivity spectrum in Fig. 1(c). Thus, at the probe laser wavelength (320 nm), we expect a linear relationship between reflectance and temperature change. To check the linearity of the measured reflectivity with temperature change, a series of thermoreflectance transients were measured for the GaN-50 nm SiN$_x$-diamond wafer by changing the average pump laser power from 3 mW to 10 mW. Figure 2(b) provides those transients, showing that they are identical within the measurement noise, verifying that the linear relationship is valid in our measurements. Secondly, it is important to verify that the modulated reflectivity signal originates from the sample surface. As was reported for the transducer-less UV/Vis-TTR technique,[17] this was achieved by comparing the measured transients to those measured from metal-transducer TTR. As depicted in the inset of Fig. 2(c), the metal-transducer TTR measurements were performed on each wafer, which was coated with a 100 nm-thick Au transducer, using a 10-nm thin Ti adhesion layer. The pump laser used is the same as that in UV/UV-TTR, while the probe is a 532 nm CW laser,

maximising the thermo-optic coefficient of Au.[21] Figures 2(c) and 2(d) compare the thermoreflectance transients measured by metal-transducer TTR and transducer-less UV/UV-TTR. The transients measured for the same wafer with two different techniques show deviation at shorter timescales (<50 ns), due to the thermal response time of the gold transducer following the pulsed heating. After 50 ns, once the transducer layer reaches thermal equilibrium with the GaN surface, the temperature transients are identical within the measurement noise, verifying that the surface temperature is measured using the UV probe laser.

The measured thermoreflectance transients, given in Fig. 2(a), are fitted using an analytical transmission-line axis-symmetric thermal transport model described in Ref. 22. This model solves the transient heat transport equation, obtaining an analytical form for the temperature rise at the surface of a multilayer material with a surface heat load. Considering that there is about 100 nm absorption (volumetric heating) in the GaN layer, it is necessary to assess the surface heat load simplification. This was done using a commercial finite element method (FEM) code (see details in the supplementary material), showing that the surface heat load simplification has a negligible effect on the result. The analytical model describes the sample surface temperature which is affected by materials' thermal conductivity, density, specific heat capacity, thickness of each layer/material, and geometrical and temporal characteristics of both pump and probe lasers. In this work, the layer thickness (Table I), material's density and specific heat capacity (literature reported values[23–32] are given in Table II) were fixed. The pump laser spot shape was measured by imaging the reflected laser intensity distribution, having a Gaussian profile with a 50 μm FWHM. Then, the remaining parameters, the TBR$_{eff}$ and thermal conductivities of GaN (k_{GaN}) and the substrate ($k_{substrate}$), are treated as variables and adjusted to fit the modelling results to the measured traces. A combined Monte-Carlo and Nelder-Mead nonlinear algorithm was used for multi-parameter fitting, as described in detail in our previous work.[33,34] Note that TBR$_{eff}$ is determined by the ratio of interlayer thickness to its fitted thermal conductivity. For the
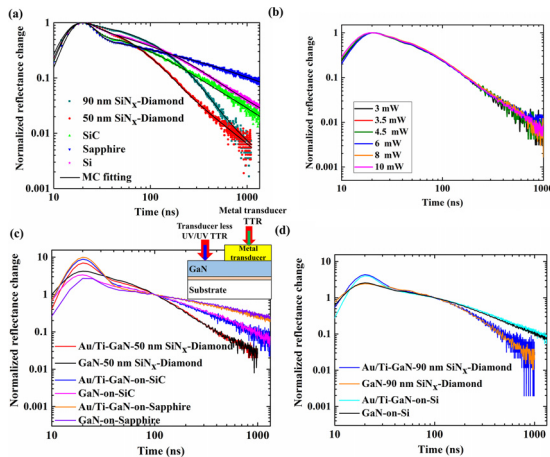

FIG. 2. (a) Thermoreflectance transients measured by transducer-less UV/UV-TTR for the wafers studied, normalized to the peak reflectivity modulation, best fitting results are overlaid. (b) A series of thermoreflectance transients measured by UV/UV-TTR on the GaN-50 nm SiN$_x$-diamond wafer by changing the pump laser power from 3 mW to 10 mW. (c) Thermoreflectance transients measured on GaN-50 nm SiN$_x$-diamond, GaN-on-SiC and GaN-on-sapphire wafers with transducer-less UV/UV-TTR, benchmarking against those measured on metal-transducer TTR, all transients normalized at 100 ns to aid visual comparison. (d) Thermoreflectance transients measured on GaN-90 nm SiN$_x$-diamond and GaN-on-Si wafers with transducer-less UV/UV-TTR, benchmarking against those measured on metal-transducer TTR.

TABLE II. Material density and specific heat capacity at 25 °C used as fixed parameters to fit the experimental data.

Layers	Specific heat capacity (J kg^{-1} K^{-1})	Density (kg m^{-3})
GaN	415[a]	6150[b]
Diamond	515[c]	3510[d]
SiC	675[e]	3210[d]
Sapphire	778[f]	3980[h]
Si	700[g]	2330[d]
AlN	730[i]	3260[j]

[a]Reference 23.
[b]Reference 24.
[c]Reference 25.
[d]Reference 26.
[e]Reference 27.
[f]Reference 28.
[g]Reference 29.
[h]Reference 30.
[i]Reference 31.
[j]Reference 32.

GaN-on-Si wafer, the SRL has an appreciable thickness and thermal impedance; so, it is not well described by a TBR$_{eff}$ value, and is better represented by an effective thermal conductivity (k_{SRL}) value. In addition, the effective heat capacity of the SRL (HC$_{SRL}$) is not known and treated as a fitting parameter. The SRL density is treated as a fixed input parameter and assumed to be the average of GaN and AlN values. For all the wafers studied, the 20–30 nm-thick AlGaN layer on the top surface was neglected in the fitting since our model results (given in Fig. S1 in supplementary material) show that it has negligible effect. The simulated peak temperature rise at the surface of GaN-50 nm SiN$_x$-diamond is 55 °C. After 20 ns, the temperature rise at the AlGaN/GaN surface reduces to 40 °C, while it is 20 °C at the GaN/TBR$_{eff}$ interface. After 100 ns, the temperature rise reduces to 20 °C and 10 °C, respectively. Thus, the measured thermal property values approximate the values at ambient temperature. The thermoreflectance transients measured with metal-transducer TTR were fitted with the same method. Note that the Au thermal conductivity and TBR$_{eff}$ at the Au/GaN interface are unknown and treated as variables in the analysis. Therefore, compared to the metal-transducer TTR, two variables are removed from the analysis in the transducer-less UV/UV-TTR measurement, decreasing the uncertainty.

Figures 3(a)–3(d) show the sensitivity of the UV/UV-TTR signal to a change of 10% in each thermal parameter for the wafers studied. This sensitivity analysis demonstrates that each parameter has an impact on the reflectivity in different timescales. This is due to the spatial and temporal evolution of heat, which diffuses from the GaN surface through the interlayer, into the substrate. Besides, the sensitive time-scales and the magnitude for the same parameter vary in different wafers. Particularly, k_{GaN} greatly impacts the measured response at approximately 30–200 ns for the GaN-on-SiC and GaN-on-sapphire. Whereas for the GaN-on-diamond and GaN-on-Si wafers, it weakly affects the response at a shorter time window, approximately 10–50 ns. The weaker sensitivity of k_{GaN} in GaN-on-diamond and GaN-on-Si wafers is due to the smaller ratio of GaN thermal resistance to TBR$_{eff}$. And, the shorter sensitive time window is owing to the less thickness of GaN layer. Considering that the detector used has a limited bandwidth (50 MHz), the measured transient within a 0–20 ns timescale, which is most relevant for the GaN layer, is convoluted with the detector response. This naturally affects the accuracy of the k_{GaN} value

obtained from the TTR traces of GaN-on-diamond and GaN-on-Si wafers. For accurate determination of the k_{GaN} in those two wafers, a higher bandwidth photodetector can be used, although there is a trade-off in signal amplification gain.

To verify this technique's accuracy, we benchmark the measured results against the data obtained from the metal-transducer TTR. Figure 4 plots the measured k_{GaN}, TBR$_{eff}$ and $k_{substrate}$ for all the wafers studied. k_{GaN} of GaN-on-SiC and GaN-on-sapphire wafers, measured by transducer-less UV/UV-TTR, is 185 and 160 W m^{-1} K^{-1} with the uncertainty of about ±15%. k_{GaN} of GaN-on-diamond and GaN-on-Si wafers is measured to be within 115–140 W m^{-1} K^{-1} with a much larger uncertainty (about ±40%). The larger uncertainty in those wafers is due to the low sensitivity and the limited bandwidth of the detector, as discussed in the sensitivity analysis. Figure 4(a) shows that k_{GaN} values measured by UV/UV-TTR are consistent with those measured by metal-transducer TTR.

TBR$_{eff}$ was measured to be 43 m^2 K W^{-1} and 23 m^2 K W^{-1}, with the uncertainty of ±11%, in the GaN-on-diamond wafers with 90 nm and 50 nm-thick dielectric interlayers. As shown in Fig. 4(b), they are consistent with results measured by the metal-transducer TTR. TBR$_{eff}$ values of GaN-on-SiC and GaN-on-sapphire wafers also match well with the results determined by metal-transducer TTR. The uncertainties are ±6.5% and ±20%, respectively. As shown in the GaN-on-sapphire sensitivity analysis [Fig. 3(d)], the TTR trace is not that sensitive to TBR$_{eff}$, owing to the low thermal resistance
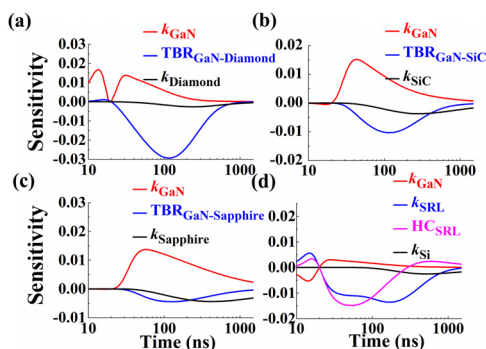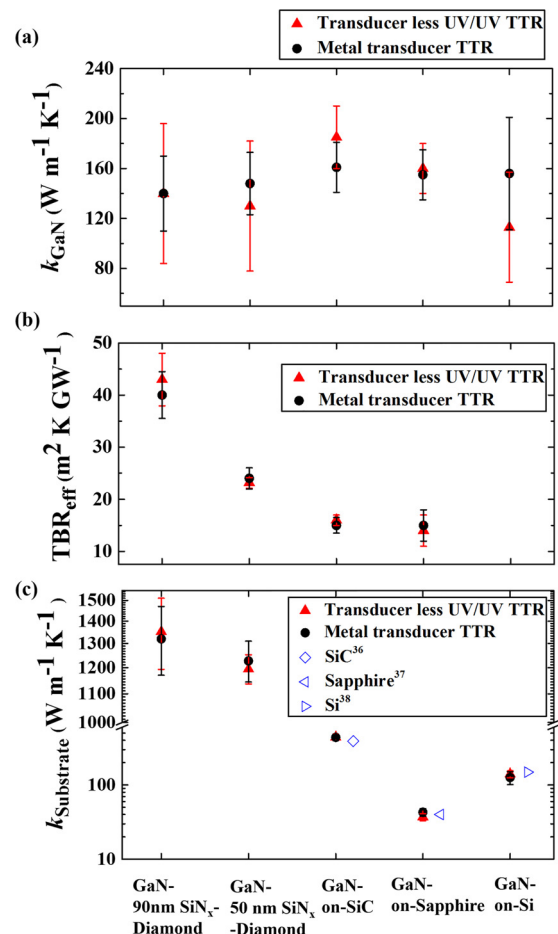

FIG. 3. Sensitivity plot (transducer-less UV/UV-TTR): thermoreflectance signal change with respect to 10% variation in each thermal parameter for (a) GaN-90 nm SiN$_x$-diamond, (b) GaN-on-SiC, (c) GaN-on-sapphire, and (d) GaN-on-Si wafers.

FIG. 4. Measured (a) k_{GaN}, (b) TBR$_{eff}$, and (c) $k_{substrate}$ for all the wafers studied, benchmarking against results measured by metal-transducer TTR.

contrast between TBR$_{eff}$ and the substrate, resulting in the lower accuracy of TBR$_{eff}$ fitting. For the GaN-on-Si wafer, the measured k_{SRL} is 8.6 ± 1 W m^{-1} K^{-1}, consistent with the data (7.8 ± 1.2 W m^{-1} K^{-1}) measured by metal-transducer TTR. The thermal conductivities of AlGaN thin films have also been assessed using the TDTR technique by Daly *et al.*[35] Al$_{0.18}$Ga$_{0.82}$N, Al$_{0.20}$Ga$_{0.80}$N and Al$_{0.44}$Ga$_{0.56}$N were reported to be 14.6, 13.4, and 6.2 W m^{-1} K^{-1}. It is shown that our measured k_{SRL} is consistent with the reported results of AlGaN thin films. In addition, the SRL effective heat capacity is fitted to be 492 ± 18 J kg^{-1} K^{-1}, located within the heat capacity of GaN (430 J kg^{-1} K^{-1})[23] and AlN (730 J kg^{-1} K^{-1}).[31]

As for the substrates (polycrystalline diamond, SiC, sapphire, and Si), as shown in Fig. 4(c), the measured thermal conductivity values are found to be comparable to the data measured by metal-transducer TTR and the reported values in the literature.[36–38] The research[39] has illustrated that for the polycrystalline diamond substrate, its thermal conductivity changes through its thickness. Therefore, the measured results are the effective thermal conductivity through its thickness.

Therefore, the measured TBR$_{eff}$ and layer thermal conductivity results match well with those measured by the standard metal-transducer TTR, showing that the technique presented here is well suited to measure the thermal properties of the semiconductor wafer, without the need for test structure fabrication or metal deposition, making this approach even suitable as a process monitoring tool in a manufacturing line.

In conclusion, a generic thermoreflectance technique was demonstrated for non-invasive thermal assessment of GaN-based wafers. The major key in this technique is that the above-bandgap lasers are carefully selected to both pump and probe the GaN surface with strong optical absorption to avoid any interferences caused by sub-surface reflections, ensuring that this technique strictly follows the fundamental principle of the thermoreflectance-based method. With the technique, we investigated and reported the interfacial thermal resistance (TBR$_{eff}$) and layer thermal conductivities of several common GaN-based wafers, including GaN-on-diamond, GaN-on-SiC, GaN-on-sapphire, and GaN-on-Si. For the GaN-on-Si wafers, the strain relief layer's thermal conductivity was measured. The measured properties are consistent with the values measured by the metal transducer TTR technique, demonstrating this technique's capability and accuracy for GaN-based wafer thermal characterization.

See supplementary material for Fig. S1 and the assessment of surface heat load simplification.

[1]M. Kuball and J. W. Pomeroy, IEEE Trans. Device Mater. Reliab. **16**, 667 (2016).
[2]X. B. Luo, R. Hu, S. Liu, and K. Wang, Prog. Energy Combust. Sci. **56**, 1 (2016).
[3]M. Kuball, J. M. Hayes, M. J. Uren, T. Martin, J. C. H. Birbeck, R. S. Balmer, and B. T. Hughes, IEEE Electron Device Lett. **23**, 7 (2002).
[4]D. Francis, F. Faili, D. Babic, F. Ejeckam, A. Nurmikko, and H. Maris, Diamond Relat. Mater. **19**, 229 (2010).
[5]J. D. Blevins, G. D. Via, K. Sutherlin, S. Tetlak, B. Poling, R. Gilbert, B. Moore, J. Hoelscher, B. Stumpff, A. Bar-Cohen, J. J. Maurer, and A. Kane, in *Proceedings of the Compound Semiconductor Manufacturing Technology Conference*, Denver, Colorado, USA, 2014, p. 105.
[6]D. Liu, D. Francis, F. Faili, C. Middleton, J. Anaya, J. W. Pomeroy, D. J. Twitchen, and M. Kuball, Scr. Mater. **128**, 57 (2017).
[7]J. W. Pomeroy, M. Bernardoni, D. C. Dumka, D. M. Fanning, and M. Kuball, Appl. Phys. Lett. **104**, 083513 (2014).
[8]C. Hodges, J. A. Calvo, S. Stoffels, D. Marcon, and M. Kuball, Appl. Phys. Lett. **103**, 202108 (2013).
[9]A. Sarua, H. Ji, K. P. Hilton, D. J. Wallis, M. J. Uren, T. Martin, and M. Kuball, IEEE Trans. Electron Devices **54**, 3152 (2007).
[10]H. Sun, R. B. Simon, J. W. Pomeroy, D. Francis, F. Faili, D. J. Twitchen, and M. Kuball, Appl. Phys. Lett. **106**, 111906 (2015).
[11]J. Cho, Z. Li, E. Bozorg-Grayeli, T. Kodama, D. Francis, F. Ejeckam, F. Faili, M. Asheghi, and K. E. Goodson, IEEE Trans. Compon., Packag., Manuf. Technol. **3**, 79 (2013).
[12]J. W. Cho, Y. Li, W. E. Hoke, D. H. Altman, M. Asheghi, and K. E. Goodson, Phys. Rev. B **89**, 115301 (2014).
[13]P. L. Komarov, M. G. Burzo, G. Kaytaz, and P. E. Raad, Microelectron. J. **34**, 1115–1118 (2003).
[14]K. E. Goodson, O. W. Käding, M. Rösler, and R. Zachai, J. Appl. Phys. **77**, 1385 (1995).
[15]O. W. Kading, H. Skurk, and K. E. Goodson, Appl. Phys. Lett. **65**, 1629–1631 (1994).
[16]R. Garrelts, A. Marconnet, and X. Xu, Nanoscale Microscale Thermophys. **19**, 245–257 (2015).
[17]J. W. Pomeroy, R. B. Simon, H. R. Sun, D. Francis, F. Faili, D. J. Twitchen, and M. Kuball, IEEE Electron Device Lett. **35**, 1007 (2014).
[18]J. F. Muth, J. H. Lee, I. K. Shmagin, R. M. Kolbas, H. C. Casey, B. P. Keller, U. K. Mishra, and S. P. DenBaars, Appl. Phys. Lett. **71**, 2572–2574 (1997).
[19]N. Watanabe, T. Kimoto, and J. Suda, J. Appl. Phys. **104**, 106101 (2008).
[20]N. A. Sanford, L. H. Robins, A. V. Davydov, A. Shapiro, D. V. Tsvetkov, A. V. Dmitriev, S. Keller, U. K. Mishra, and S. P. DenBaars, J. Appl. Phys. **94**, 2980 (2003).
[21]R. B. Wilson, B. A. Apgar, L. W. Martin, and D. G. Cahill, Opt. Express **20**, 28829 (2012).
[22]P. Hui and H. S. Tan, IEEE Trans. Compon., Packag., Manuf. Technol., Part B **17**, 426 (1994).
[23]K. T. Jacob, S. Singh, and Y. Waseda, J. Mater. Res. **22**, 3475 (2007).
[24]H. Harima, J. Phys.: Condens. Matter **14**, R967–R993 (2002).
[25]A. C. Victor, J. Chem. Phys. **36**, 1903 (1962).
[26]G. A. Slack, J. Appl. Phys. **35**, 3460 (1964).
[27]O. Nilsson, H. Mehling, R. Horn, J. Fricke, R. Hofmann, S. G. Müller, R. Eckstein, and D. Hofmann, High Temp.-High Pressures **29**, 73 (1997).
[28]D. A. Ditmars, S. Ishihara, S. S. Chang, G. Bernstein, and E. D. West, J. Res. Natl. Bur. Stand. **87**, 159 (1982).
[29]H. R. Shanks, P. H. Sidles, P. D. Maycock, and G. C. Danielson, Phys. Rev. **130**, 1743 (1963).
[30]D. C. Harris, *Materials for Infrared Windows and Domes: Properties and Performance* (SPIE, Washington, 1999).
[31]R. B. Dinwiddie, A. J. Whittaker, and D. G. Onn, Int. J. Thermophys. **10**, 1075 (1989).
[32]G. A. Slack, J. Phys. Chem. Solids **34**, 321 (1973).
[33]Y. Zhou, R. Ramaneti, J. Anaya, S. Korneychuk, J. Derluyn, H. Sun, J. Pomeroy, J. Verbeeck, K. Haenen, and M. Kuball, Appl. Phys. Lett. **111**, 041901 (2017).
[34]Y. Zhou, J. Anaya, J. Pomeroy, H. Sun, X. Gu, A. Xie, E. Beam, M. Becker, T. A. Grotjohn, C. Lee, and M. Kuball, ACS Appl. Mater. Interfaces **9**, 34416–34422 (2017).
[35]B. C. Daly, H. J. Maris, A. V. Nurmikko, M. Kuball, and J. Han, J. Appl. Phys. **92**, 3820 (2002).
[36]J. W. Cho, E. Bozorg-Grayeli, D. H. Altman, M. Asheghi, and K. E. Goodson, IEEE Electron Device Lett. **33**, 378 (2012).
[37]E. R. Dobrovinskaya, L. A. Lytvynov, and V. Pishchik, *Sapphire-Material, Manufacturing, Applications* (Springer-Verlag, New York, 2009).
[38]C. J. Glassbrenner and G. A. Slack, Phys. Rev. **134**, A1058 (1964).
[39]J. Anaya, H. Sun, J. W. Pomeroy, and M. Kuball, in *IEEE Intersociety Thermal and Thermomechanical Conference*, Las Vegas, Nevada, USA, 2016, p.1558.